Applied Surface Science 562 (2021) 149996

Contents lists available at ScienceDirect

Applied Surface Science

journal homepage: www.elsevier.com/locate/apsusc

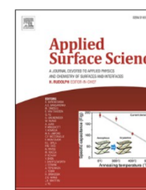

Full Length Article

Vapor-phase grafting of a model aminosilane compound to Al_2O_3, ZnO, and TiO_2 surfaces prepared by atomic layer deposition

Vepa Rozyyev [a,b,d], Julia G. Murphy [b,c], Edward Barry [a,b], Anil U. Mane [b], S.J. Sibener [b,c], Jeffrey W. Elam [a,b,*]

[a] *Applied Materials Division, Argonne National Laboratory, Lemont, IL 60439, USA*
[b] *Advanced Materials for Energy-Water Systems (AMEWS), Energy Frontier Research Center (EFRC), Lemont, IL 60439, USA*
[c] *The James Franck Institute and Department of Chemistry, The University of Chicago, 929 E. 57th Street, Chicago, IL 60637, USA*
[d] *Pritzker School of Molecular Engineering, The University of Chicago, 5640 S. Ellis Ave, Chicago, IL 60637, USA*

ARTICLE INFO

Keywords:
Atomic layer deposition
Self-assembled monolayer
Aminosilane
Metal oxide
Surface functionalization

ABSTRACT

Atomic layer deposition (ALD) is a highly versatile surface functionalization technique that can conformally coat both planar and porous substrates. Here we use ALD metal oxide layers to establish a well-defined starting surface for vapor-phase surface organic modification. Vapor-phase (3-aminopropyl)triethoxysilane (APTES) surface silanization of ALD Al_2O_3, ZnO and TiO_2 surfaces were studied at 100 °C, 150 °C and 200 °C. In situ quartz crystal microbalance (QCM) and Fourier-transform infrared (FTIR) spectroscopy measurements, and ex situ atomic force microscopy (AFM) and X-ray photoelectron spectroscopy (XPS) measurements showed uniform monolayer silane formation through self-limiting APTES reaction. We observed a higher surface density of grafted APTES species following silanization at 100 °C compared to 200 °C, and we attribute this to the temperature-dependent reactivity of the surface hydroxyls and changes in the mode of APTES reaction. The FTIR and XPS measurements revealed that APTES reacts with Al_2O_3 and ZnO exclusively through metal siloxy bond formation. However, APTES reacts with TiO_2 through both siloxy bond formation and ammonium salt formation via the amine group.

1. Introduction

Water contamination from a variety of different sources poses a significant risk to human health. Among the various water treatment technologies, selective adsorption is a promising method due to its simplicity and cost efficiency. Commercial adsorbent materials such as activated carbons, clays, and zeolites perform acceptably in a subset of cases, but lack the selective surface adsorption sites necessary for effective removal of some contaminants, especially challenging pollutants such as perfluoroalkyl substances (PFAS) [1]. To address these challenges and enable the design of robust, effective sorbents, fundamental studies of the synthesis and characterization of model adsorption sites with well-defined structure and chemistry are essential. Among the possible substrates for preparing selective adsorption sites, metal oxides are chemically and thermally robust, low cost, and easily prepared as porous slabs, micro- or nanoscale powders, and porous solids in large quantities [3–5]. Surface modification of such materials with organic species is an ideal way to tailor the surface properties for applications such as water treatment, sensors, gas capture and drug delivery [6–9]. In addition to bulk oxides, most metal and semiconducting materials are terminated with a thin native oxide layer. Virtually all metal oxide surfaces (bulk and thin film) are covered with hydroxyl (OH) species. Silanization of the hydroxylated surface can impart a wide array of chemical functionalities (e.g. hydrophobiciy, oleophilicity, electrostatic charge), or prepare the surface for further chemical treatment by creating stable siloxy bonds between the oxygen atom of the OH group and the silicon atom of the silanization agent [10].

Because of its bifunctional nature, low cost, and reactivity, (3-aminopropyl)triethoxysilane (APTES) is a widely used silanization agent for modifying the surfaces of hydroxylated glass and silica [6,11,12]. While the ethoxy group of APTES reacts with hydroxyl groups of the substrate surface, the amine group at the opposite end of the APTES molecule can be used as a chelation agent or linker to allow further functionalization. APTES silanization is performed both in solution and in the gas phase. In solution-phase silanization, trace amounts of water in the solvent can lead to the self-polymerization of APTES leading to the formation of

* Corresponding author.
E-mail address: jelam@anl.gov (J.W. Elam).

https://doi.org/10.1016/j.apsusc.2021.149996

irregular, multilayer films [13]. In addition, solution phase silanization with APTES is sensitive to many factors such as solvent composition, temperature, reaction time, concentration, and post treatment steps [13]. However, self-polymerization is much less problematic in the vapor phase silanization of APTES due to the negligible vapor pressures of the APTES oligomers. As a consequence, it is much easier to create uniform APTES monolayers using vapor phase silanization compared to solution phase silanization [10,14–16].

The APTES ethoxy groups can react with hydroxyls on a metal oxide surface (M—OH) by condensation to form one, two, or three siloxy (M—O—Si) bonds and release ethanol. Alternatively, proton transfer from a surface hydroxyl to the APTES amine group can form an ammonium cation and an oxygen anion leading to ionic bonding between APTES and the metal oxide surface. These different modes for APTES to react with surface hydroxyl groups are shown schematically in Fig. 1a and are described by the following chemical equations:

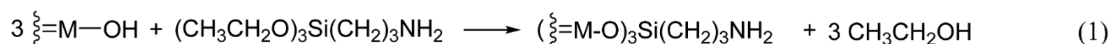

$$3\ \text{≀=M—OH} + (CH_3CH_2O)_3Si(CH_2)_3NH_2 \longrightarrow (\text{≀=M-O})_3Si(CH_2)_3NH_2 + 3\ CH_3CH_2OH \quad (1)$$

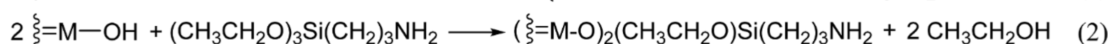

$$2\ \text{≀=M—OH} + (CH_3CH_2O)_3Si(CH_2)_3NH_2 \longrightarrow (\text{≀=M-O})_2(CH_3CH_2O)Si(CH_2)_3NH_2 + 2\ CH_3CH_2OH \quad (2)$$

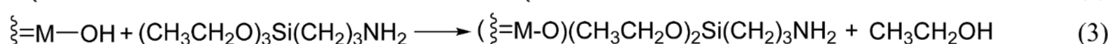

$$\text{≀=M—OH} + (CH_3CH_2O)_3Si(CH_2)_3NH_2 \longrightarrow (\text{≀=M-O})(CH_3CH_2O)_2Si(CH_2)_3NH_2 + CH_3CH_2OH \quad (3)$$

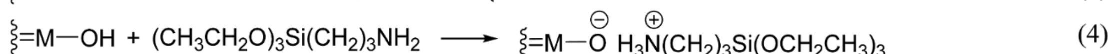

$$\text{≀=M—OH} + (CH_3CH_2O)_3Si(CH_2)_3NH_2 \longrightarrow \text{≀=M—}\overset{\ominus}{O}\ H_3\overset{\oplus}{N}(CH_2)_3Si(OCH_2CH_3)_3 \quad (4)$$

In Eq. (1), the APTES molecule reacts with three surface hydroxyl groups to release three ethanol molecules and create three siloxy bonds. Similarly, Eqs. (2) and (3) describe the reaction of two and one APTES ethoxy groups with surface hydroxyls, respectively. Finally, Eq. (4) shows the reaction of the APTES amine group with a surface hydroxyl to form an ionic bond.

When APTES reacts through siloxy bonds, it is challenging to accurately measure the number of ethoxides that have reacted with surface hydroxyls. Once the surface is exposed to ambient humidity or trace water in solution, unreacted ethoxy groups can hydrolyze to form siloxane (Si—O—Si) linkages that are difficult to differentiate from siloxy linkages. In addition, even if the unreacted ethoxy groups are preserved, it can be difficult to measure their concentration using elemental analysis such as X-ray photoelectron spectroscopy (XPS) due to interference from adventitious carbon that contaminates the surface through air exposure during sample transfer. These difficulties can complicate the task of identifying the APTES surface structures (Fig. 1a). However, in situ measurements can overcome these difficulties by eliminating the loss of ethoxy groups through hydrolysis and surface contamination by adventitious carbon allowing the structure of the APTES monolayer to be deduced.

Although APTES has been extensively studied for the functionalization of silicon dioxide, there are relatively few reports on the surface modification of other metal oxides such as aluminum oxide (Al_2O_3), titanium dioxide (TiO_2) and zinc oxide (ZnO), and their reaction mechanisms are not well understood [17–19]. Using atomic layer deposition (ALD), uniform thin films of virtually any metal oxide, including Al_2O_3, TiO_2 and ZnO, can easily be deposited on a wide range of substrate materials [20]. ALD uses sequential, self-limiting surface reactions allowing conformal metal oxide films to be deposited on both planar surfaces and porous media, and this capability facilitates systematic study of APTES vapor phase grafting on these metal oxide surfaces [20–22]. In this manuscript, we report a detailed study of APTES vapor-phase grafting on ALD Al_2O_3, TiO_2 and ZnO surfaces. We employ in situ quartz crystal microbalance (QCM) and in situ Fourier Transform Infrared (FTIR) spectroscopy measurements to monitor the

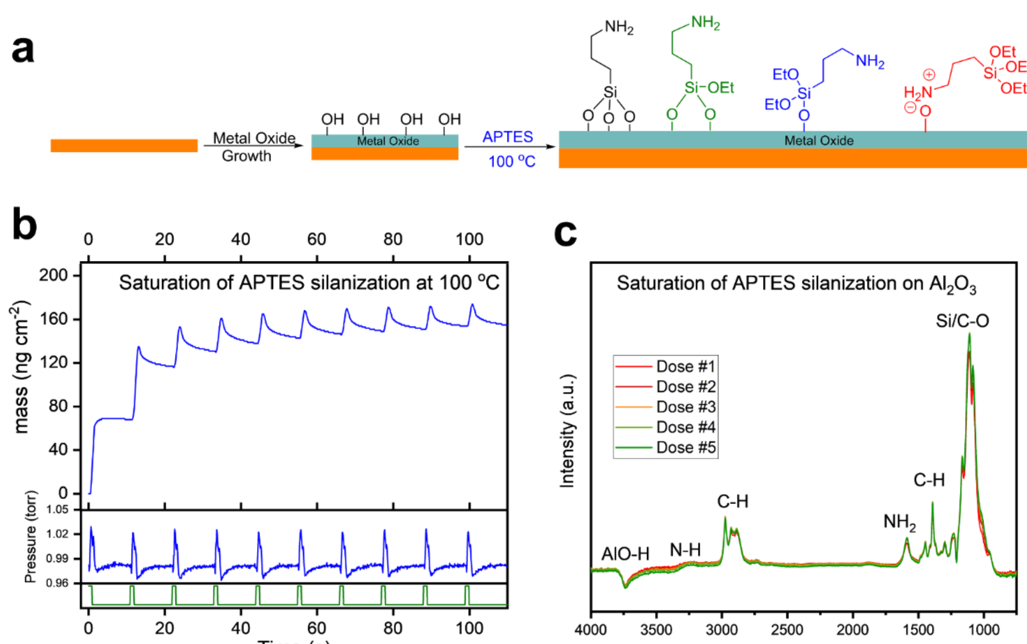

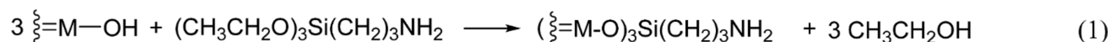
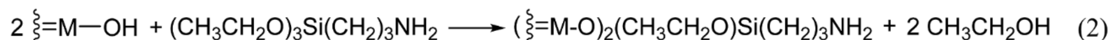
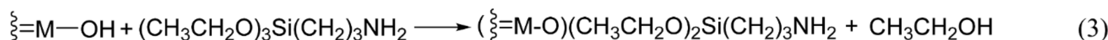
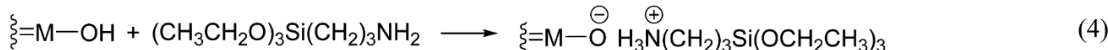

reaction of APTES on the ALD metal oxide surfaces as well as the subsequent vapor phase hydrolysis of the grafted APTES species. In addition, we prepared ALD Al_2O_3, TiO_2 and ZnO coatings on silicon coupons, subjected them to APTES vapor phase grafting, and examined the samples using atomic force microscopy (AFM) and X-ray photoelectron spectroscopy (XPS).

2. Experimental methods

2.1. Materials

(3-aminopropyl)triethoxysilane (APTES) (99%) was purchased from Sigma Aldrich and used as received. Trimethylaluminum (98%), titanium tetrachloride (99%), and diethylzinc (95%) were purchased from Strem Chemicals, Inc. The HPLC grade water was purchased from Sigma Aldrich and used without further purification. The zirconium oxide nanoparticles (~20 nm, diameter) used in the FTIR measurements were purchased from US Research Nanomaterials Inc. All vapor phase reactions were done under inert conditions using ultrahigh purity N_2 (UHP, 99.999%).

2.2. Gas phase deposition and APTES reaction

The Growth of Al_2O_3, ZnO TiO_2 were performed in a hot-wall viscous flow ALD reactor that is described in detail in another study [23]. Ultrahigh purity N_2 was used as a carrier gas with a total mass flow rate of 225 sccm and a background pressure of 0.9–1 Torr. The temperature of the reactor was maintained by proportional-integral–differential temperature controllers with an accuracy of ±0.03 °C. Metal oxide films were deposited through self-limiting binary ALD reactions. TMA, DEZ and $TiCl_4$ were used as precursors for the metal sources, and water was used as the oxygen precursor. For each ALD cycle, 1 s dose of metal precursor, 10 s of carrier gas purging, 1 s dose of water, and 10 s of carrier gas purging was performed sequentially (1 s:10 s:1s:10 s). The TMA, DEZ, $TiCl_4$ and water were kept at room temperature. During reactant dosing, the partial pressures of TMA, DEZ and water were approximately 0.2 Torr, and the partial pressure of $TiCl_4$ was about 0.05 Torr as measured using a Baratron capacitance manometer. Silanization was performed on these films in the same reactor, at the same temperature, and immediately following the metal oxide ALD. Silanization used multiple cycles of 1 s dose of APTES and 10 s of carrier gas purging (1 s:10 s). The APTES was heated to 100 °C in a stainless-steel bubbler to achieve a vapor pressure of about 0.05 Torr. The metal oxide ALD and subsequent silanization were carried out at three different temperatures of 100 °C, 150 °C and 200 °C.

2.3. In situ QCM studies

The metal oxide ALD and APTES silanization were monitored with in situ quartz crystal microbalance (QCM) measurements. The single-side polished 6 MHz RC-cut quartz sensor (Philip Technologies) was mounted in a Maxtek BSH-150 sensor head and installed in the middle of the 2″ diameter stainless steel flow tube of the ALD reactor. The QCM can experiment, ~20 Al_2O_3 ALD cycles of TMA/H_2O were performed to prepare a well-defined starting surface and to confirm the expected growth per cycle value of ~40 ng cm^{-2} [23].

2.4. X-ray photoelectron spectroscopy (XPS)

The XPS measurements were carried out on a Thermo Fisher k-Alpha+ and the spectra were analyzed using Thermo Fisher Avantage software. All the spectra were referenced to the C1s peak at 284.8 eV. The samples were prepared on copper foil by performing 100 cycles of metal oxide ALD followed by silanization. The copper foil eliminated sample charging artifacts that are typically observed using insulating substrates, and was first cleaned with methanol and acetone, then dried using flowing N_2 gas. After loading the substrate samples into the ALD reactor, the reactor was allowed to equilibrate for 15 min under reaction conditions (temperature, carrier gas flowing at 225 sccm at 1 Torr) to stabilize the temperature and dry the substrates.

2.5. In situ transmittance absorbance Fourier-transform infrared (FTIR) spectroscopy

The in situ FTIR was performed using a Nicolet 6700 FTIR (Thermo Scientific) spectrometer that was connected to an ALD reactor. Each FTIR spectrum was measured as an average of 256 scans in the spectral range of 4000–400 cm^{-1}. The samples were prepared on a steel mesh by pressing ZrO_2 nanoparticles (20 nm, US Research Nanomaterials) to the grid. The ZrO_2 nanoparticles were chosen as a substrate because they have high transparency in the spectral range of 4000–800 cm^{-1}. Furthermore, the high surface area of nanoparticles in comparison to planar substrates provide a greater IR absorption intensity. The commercial grids were purchased from Fotofab, Inc. with a thickness of 50 μm. After loading the samples into the FTIR reactor, the samples were allowed to equilibrate for 30 min under reaction conditions before the deposition of metal oxides. After equilibration, 10 cycles of metal oxide ALD were performed and the reaction progress was monitored by FTIR after each half ALD cycle. Following the metal oxide ALD, silanization was carried out by dosing APTES. FTIR spectra were recorded after each exposure (5 s APTES dosing, 60 s carrier gas purging) until no change was observed in the spectra indicating saturation of the silanization reaction. After silanization, the attached silane groups on the sample surface were reacted with water (5 s H_2O dosing, 60 s carrier gas purging), and spectra were recorded after each water exposure until no change was observed in the spectra indicating saturation of the water reaction.

2.6. Atomic force microscopy (AFM)

The AFM imaging was conducted with an Asylum Research Cypher ES Environmental AFM. High-speed, tapping-mode imaging was performed with gold-coated Asylum Research FS1500-AuD cantilevers with a resonant frequency of 1.5 MHz. Images were collected at room temperature with a 500 or 800 mV set point, selected to prevent tip-induced sample damage. The AFM data were processed using a first order flat-

by silanization using APTES. Prior to coating, the Si (1 0 0) coupons were first cleaned with methanol and acetone, and then dried with flowing N_2 gas. After loading the substrate samples into the reactor, it was allowed to equilibrate for 15 min at reaction conditions (temperature, carrier gas flowing at 225 sccm at 1 Torr) to stabilize the temperature and dry the samples.

3. Results and discussion

3.1. The APTES reaction on Al_2O_3

We performed in situ QCM measurements to monitor both the metal oxide ALD and the APTES vapor phase grafting reactions. Prior to each QCM measurement, the QCM sensor was first coated with ALD Al_2O_3 using ~20 ALD cycles of TMA and H_2O to prepare a consistent starting surface. The Al_2O_3 ALD using TMA and H_2O has been extensively studied and is well-understood [20]. Fig. S18a shows that the QCM mass increases in a stepwise fashion during each TMA and H_2O exposure with a net mass change of 36 ng cm^{-2} per cycle. This value is similar to previous measurements of Al_2O_3 ALD at 100 °C [24]. The Fig. 1b shows in situ QCM measurements recorded during APTES exposure to the ALD Al_2O_3 surface. The upper trace shows the QCM signal, the middle trace shows pressure, and the lower trace shows the status of the APTES dosing valve. APTES silanization was performed using 1 s APTES exposures and 10 s of inert gas purging (1 s APTES:10 s N_2). The mass increases during the initial 4–5 1 s APTES doses but remains essentially constant at 140 ng cm^{-2} during subsequent APTES doses indicating saturation of the silanization reaction on the hydroxylated ALD Al_2O_3 surface. Fig. 1b shows a transient increase and slow decay in the QCM signal appearing during each APTES dose. We attribute this transient behavior to the physisorption and subsequent desorption of APTES from the surface.

The in situ FTIR spectra are presented as difference spectra where the previously recorded spectrum is subtracted from the current spectrum before plotting the data. Consequently, positive peaks indicate new species created during the precursor exposure and negative peaks result from the consumption of surface species. The Fig. 1c shows in situ FTIR measurements recorded during exposure of the ALD Al_2O_3 surface to APTES vapor. APTES reacts with surface Al_2O_3 hydroxyls to produce a negative OH stretching band at 3730 cm^{-1} indicating the consumption of Al-OH groups. New peaks appear due to N—H stretching at 3265 cm^{-1} and bending at 1580 cm^{-1}, C—H stretching at 2900 cm^{-1} and bending at 1300 cm^{-1}, and Si/C—O at 1000–1200 cm^{-1} in agreement with previous IR measurements of aminosilane species [25]. Most of the spectral changes in Fig. 1c occur during the first APTES exposure and subsequent APTES doses have only a minor effect on the FTIR absorption. This indicates saturation of the APTES silanization reaction on the ALD Al_2O_3 surface.

Fig. S23 shows AFM images recorded following 100 metal oxide ALD cycles (a–c) and after a saturating APTES exposure on the metal oxide ALD surfaces (d–f) prepared on Si (1 0 0) substrates. The silicon wafer substrate had an RMS roughness of 0.105 nm. Prior to APTES silanization, the ALD metal oxide surfaces had RMS roughness values of 0.106 nm for Al_2O_3, 0.107 nm for TiO_2 and 0.578 nm for ZnO. After silanization, the samples showed RMS roughness values of 0.166 nm for Al_2O_3, 0.142 nm for TiO_2 and 0.798 nm for ZnO. The AFM images do not show any observable agglomerates and the RMS roughness remains approximately the same after the APTES reaction, indicating uniform silanization. There RMS roughness varies among the different ALD metal oxides. A previous AFM study reported that 600 ALD cycles of Al_2O_3 and ZnO prepared at 177 °C showed RMS roughness values of 0.25 nm, and 2.16 nm respectively [26]. For 860 cycles of ALD TiO_2 prepared at 120 °C, previous measurements yielded an RMS roughness of 0.24 nm [27]. These values are in good agreement with our measurements.

Next, we studied the effect of temperature on the APTES grafting reaction on ALD Al_2O_3. We performed the Al_2O_3 ALD and APTES silanization at 100 °C, 150 °C and 200 °C. The Al_2O_3 ALD used the timing sequence (1 s TMA:10 s N_2:1s H_2O:10 s N_2) and the APTES silanization

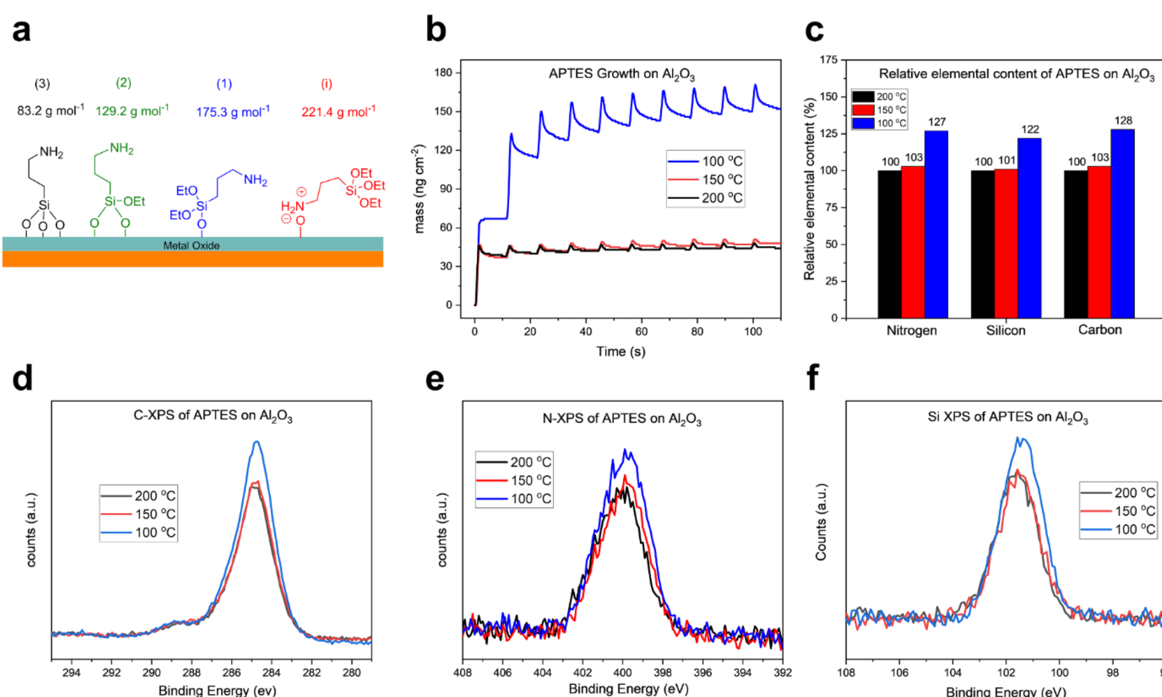

Table 1
In situ QCM measurements of mass gains during APTES reaction and mass losses during water exposures. Average and standard deviation values are calculated from three measurements for each sample. Detailed QCM mass change profiles are shown in Figs. S2–S15.

Oxide	Temperature (°C)	APTES reaction QCM Mass (ng cm^{-2})		Water reaction of surface APTES (ng cm^{-2})	
		Average	SD (σ)	Average	SD (σ)
Al_2O_3	100	151.3	3.30	−17.7	0.5
Al_2O_3	150	48.7	0.5	−5.5	1.7
Al_2O_3	200	46.7	1.9	−7	0.8
ZnO	100	93.7	4.1	−11.5	0.5
ZnO	200	53.7	1.7	−3.7	0.9
TiO_2	100	85.7	4.6	−5.3	1.7
TiO_2	200	45.7	4.9	−8	2.4

was performed using 1 s dosing of APTES and 10 s of inert gas purging (1 s APTES:10 s N_2). The APTES silanization reaction was found to saturate at all the reaction temperatures (Fig. 2b). At 150 °C and 200 °C, 90% of the saturated mass value was obtained after only a single 1 s dose of APTES. However, at 100 °C it took approximately five 1 s doses to achieve 90% of the saturated value, showing that the silanization reaction is slower at lower temperatures. The slower reaction at lower temperature is in accordance with the Arrhenius equation for chemical reaction rates.

QCM measurements of the APTES silanization reaction on Al_2O_3 revealed that at 100 °C ~150 ng cm^{-2} mass gain was observed, while at 150 °C and 200 °C only ~50 ng cm^{-2} mass gains were observed (Fig. 2b and Table 1). To understand the origin of this behavior, we performed X-ray photoelectron spectroscopy (XPS) measurements on samples prepared on copper foils using 100 Al_2O_3 ALD cycles and 10 APTES exposures of 1 s at 100 °C, 150 °C and 200 °C. Fig. 2d-2f show the high resolution XPS scans for the C 1s, N 1s and Si 1s peaks, respectively, for each of the samples. Fig. 2c plots the relative integrated XPS signals for the C 1s, N 1s and Si 1s peaks where the data for each element has been scaled to be 100 for the sample prepared at 200 °C. The XPS data reveal that samples prepared at 100 °C contain only about 27% extra nitrogen and 22% extra silicon as compared to the 200 °C values (Fig. 2c) despite the fact that the QCM mass increase is ~300% greater at 100 °C compared to 200 °C (Fig. 2b). The QCM mass changes will depend on the surface density of grafted APTES species as well as the mode of APTES bonding to the hydroxylated surface (Fig. 2a). For instance, three-anchored bonding APTES will add 83 g mol^{-1} while one-anchored bonding will add 175 g mol^{-1} (Fig. 2a). The APTES bound through the terminal nitrogen (structure (i) in Fig. 2a) will add 221 g mol^{-1} and show a distinct nitrogen XPS peak as compared to the other structures in Fig. 2a [13]. The nitrogen XPS spectrum of APTES grafted to Al_2O_3 in Fig. 2f shows only a single peak at 400 eV that we assign to the RNH_2 nitrogen of APTES [25]. This eliminates the possibility of ionic binding through the RNH_3X ammonium salt, because ammonium nitrogen would appear at a higher binding energy in XPS [28]. However, to determine the exact mode of APTES bonding (i.e. structures (1)-(3) in Fig. 2a), we first need to know the number of surface hydroxyls that react with APTES at each temperature.

In the uniform monolayer silanization of metal oxide surfaces, alkoxysilanes only react with surface hydroxyl (OH) groups. Different metal oxide surfaces have different OH surface densities for a given treatment temperature. For instance, amorphous SiO_2 has 2.35–4.6 OH nm^{-2} following treatment at temperatures of 400–190 °C [29]. The OH surface density and reactivity will dictate the monolayer silane reagent coverage. To the best of our knowledge, this has not been addressed in the literature. In order to determine the average number of OH groups that react with each APTES molecule, we performed in situ FTIR spectroscopy measurements of the ALD Al_2O_3 surface before and after the APTES grafting reaction. Before the APTES grafting, the Al_2O_3 shows a broad AlO—H stretching peak extending from 3200 to 3800 cm^{-1}. Following a saturating APTES exposure, the FTIR spectrum shows a negative AlO—H stretching feature signaling the consumption of AlO—H (Fig. 1c). The AlO—H feature partially overlaps the NH_2 stretching features at 3265 cm^{-1}. To avoid any error associated with the NH_2 peak, we confined our analysis of the AlO—H stretching feature to the range 3800–3600 cm^{-1} (Figs. S16–S17 and Table S1). By comparing the integrated areas of the AlO—H before and after APTES exposure, we found that at 200 °C about 75% of the Al_2O_3 surface hydroxyls react with APTES (Table 2). However, at 100 °C only 63% of the surface OHs reacted with APTES, which might be due to a lower OH reactivity at lower temperatures or to steric effects from unreacted ethoxides.

Al_2O_3 ALD has been extensively studied and the OH surface density has been reported [30] (Table 2). Using reported OH densities and the percentage of OHs reacted as determined by in situ FTIR measurements, we calculated the expected mass increase for each type of APTES bonding mode in Fig. 2a (Table 2). At 200 °C for 75% OH reactivity, three-anchored APTES bonding will add 34.7 ng cm^{-2} and two-anchored bonding will add 80.9 ng cm^{-2}. The in situ QCM measurements for APTES grafting at 200 °C yielded a 46.7 ng cm^{-2} mass increase indicating a mixture of three anchored and two anchored APTES bonding modes as shown in Fig. 2a. However, at 100 °C for 63% OH reactivity, the in situ QCM measurements showed a mass increase of 151.3 ng cm^{-2} suggesting a mixture of one- and two-anchored APTES bonding (Fig. 2a). These results suggest that the larger mass increase at 100 °C is due to the greater number of unreacted ethoxides at 100 °C as well as about 27% more grafted APTES molecules at 100 °C revealed from XPS elemental analysis (Fig. 2c).

In order to test our hypothesis for the greater mass increase during APTES grafting at 100 °C compared to 150 °C and 200 °C, we analyzed the in situ FTIR spectra following APTES adsorption on Al_2O_3 at different temperatures. Fig. 3a and b show FTIR difference spectra in the high and low frequency regions, respectively, following saturating APTES exposures to hydroxylated Al_2O_3 surfaces at 100 °C (black) and 200 °C (blue). Because these spectra were recorded from different powder samples which likely have different surface areas, the data were scaled by the integrated AlO—H stretching feature measured following Al_2O_3 ALD for each sample. At both temperatures, the spectra show consumption of AlO—H and formation of C—H, N—H, C—N and Si-OR/M bands indicating APTES reaction with AlO—H. The presence of strong asymmetric CH_3 stretching bands at 2970 cm^{-1}, CH_3 bending at 1390 cm^{-1} and Si—OC stretching at 1100–1200 cm^{-1} confirm the presence of unreacted ethoxide ligands at both temperatures. However, at 100 °C

Table 2
Surface OH reactivity and comparison of calculated mass increases and measured QCM data.

Substrate	Temperature (°C)	Surface OH density (nmol cm^{-2})	% of OH reacted[c]	QCM mass (ng cm^{-2})	Calculated mass increase of different structures			
				Average	(3)	(2)	(1)	(i)
Al_2O_3	100	1.66[a]	62.55%	151.3	28.8	67.1	182.0	230.0
Al_2O_3	200	1.44[a]	75.42%	46.7	34.7	80.9	219.4	277.3
ZnO	100	1.36[b]	50.23%	93.7	18.95	44.15	119.8	151.4

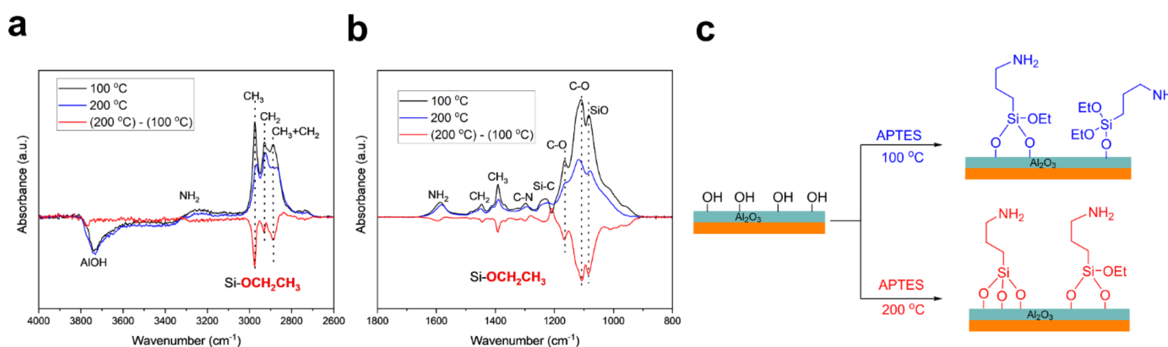

Fig. 3. (a, b) FTIR spectra following APTES grafting on hydroxylated Al_2O_3 surfaces at 100 °C (black) and 200 °C (blue). The red spectra are obtained by subtracting the 100 °C spectra from the 200 °C spectra. (c) Reaction scheme of APTES grafting on hydroxylated Al_2O_3 at 100 °C and 200 °C.

these bands are much stronger in intensity, indicating a larger number of unreacted ethoxides at 100 °C consistent with the in situ QCM measurements. To highlight these differences, the difference spectra are shown in red in Fig. 3a and 3b, and result from subtracting the 100 °C spectra from the corresponding 200 °C spectra. The negative features in the red spectra indicate the larger number of remaining ethoxide ligands following APTES grafting at 100 °C. In addition, the slightly larger NH_2 stretching band (3265 cm^{-1}) and NH_2 bending band (1590 cm^{-1}) at 100 °C indicate a higher density of grafted APTES molecules compared to 200 °C consistent with the XPS measurements (Fig. 2c). The schematic structures in Fig. 3c summarize the results from the in situ QCM, in situ FTIR and XPS measurements. We note that the in situ QCM and FTIR measurements do not unambiguously predict the mixture of grafted APTES species since a variety of linear combinations can yield the same experimental mass increase and FTIR intensity values. However, by assuming the structures shown in Fig. 3c, the number of aminosilane molecules attached to the Al_2O_3 surface were estimated from QCM, FTIR and XPS data. At 100 °C, an average of 5.42 aminosilane molecules nm^{-2} grafted to the ALD Al_2O_3 surface.

3.2. The H_2O reaction on APTES-terminated Al_2O_3

In the absence of water, unreacted ethoxide ligands remain following APTES grafting on hydroxylated Al_2O_3. However, once the surface is exposed to air the ethoxides are likely to react with water and the chemistry of the surface will change. To study this process, we exposed the surfaces to multiple doses of water at the respective temperatures and monitored the changes using in situ QCM and FTIR measurements. As expected, the QCM measurements registered a mass loss following water exposure due to hydrolysis, which replaces the heavier ethoxide groups with lighter hydroxyl groups (Fig. 4d and Table 1). The mass loss is greater at 100 °C compared to 200 °C, likely reflecting the greater number of unreacted ethoxides at 100 °C. To explore the mechanism for this reaction, we conducted in situ FTIR measurements. Water was dosed and after each dose FTIR spectra were recorded until no further changes in the spectra were observed. Fig. 4b and c show the FTIR spectra recorded in the high and low frequency regions, respectively, following saturation H_2O exposures to the APTES terminated Al_2O_3 surface at 100 °C. Similarly, Fig. 4e and 4f show the FTIR spectra following saturation

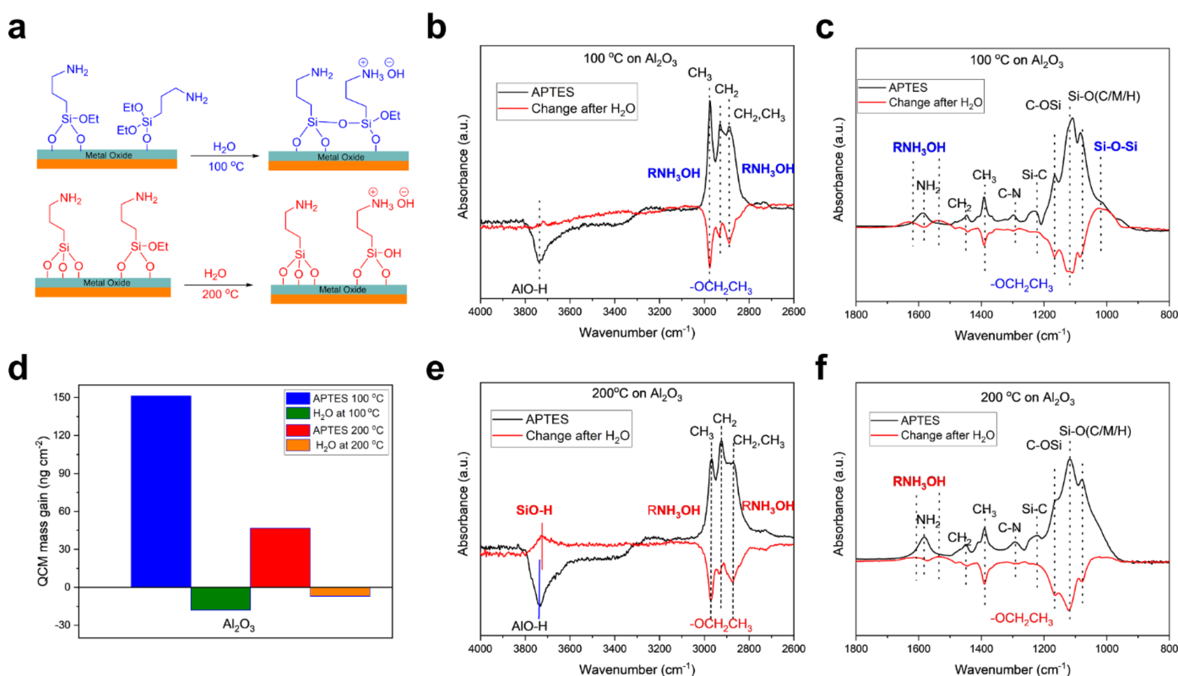

H_2O exposures to the APTES terminated Al_2O_3 surface at 200 °C. In these figures, the black traces show the FTIR spectra following APTES exposures, and the red traces show the FTIR difference spectra following H_2O exposures. At both temperatures, the FTIR measurements reveal a loss of ethoxides, through the decrease in the intensity of CH_3 and CH_2 stretching bands at 2800–3000 cm^{-1}, the CH_3 and CH_2 bending bands at 1390 and 1445 cm^{-1}, and the Si—OC bands in the range of 1100–1200 cm^{-1}. At 200 °C, the strong asymmetric CH_3 stretching band at 2970 cm^{-1} almost disappears after H_2O reaction indicating nearly complete hydrolysis of the ethoxides. However, at 100 °C the presence of a residual CH_3 stretching band shows that some of the ethoxides remain on the surface following the H_2O exposure. This may indicate a lower H_2O reactivity at 100 °C compared to 200 °C. Following H_2O reaction at 100 °C, a strong broad band appears at ~1020 cm^{-1} which can be ascribed to Si—O—Si stretching. This suggests that H_2O reacts with neighboring APTES species to form siloxane bonds as shown in Fig. 4a. As demonstrated in the previous section, some of the APTES reacts with the hydroxylated Al_2O_3 at 100 °C to form only a single Si—O—Al bond. This bonding configuration likely provides rotational freedom allowing the APTES to reorient and form siloxane bonds with adjacent APTES molecules during the H_2O exposure. However, at 200 °C we do not see evidence for Si—O—Si bond formation upon H_2O exposure (Fig. 4f). Instead, a new peak appears at ~3720 cm^{-1}, which can be ascribed to SiO—H stretching (Fig. 4e). It is interesting to note that we do not see the SiO—H stretching feature appear following H_2O exposure at 100 °C (Fig. 4b). As we have shown above, APTES reacts with the hydroxylated Al_2O_3 surface at 200 °C to form a mixture of 3- and 2-anchored species (Fig. 3c) that are rotationally restricted. Consequently, these species are not able to reorient to form siloxane bridges during the H_2O exposures and the hydrolyzed product SiO—H was formed.

In addition to the features described above, H_2O exposure at both temperatures creates new bands at 1540 cm^{-1} and 1630 cm^{-1} and a broad peak starting from 3600 cm^{-1} extending to 2600 cm^{-1} (Fig. 4b, c, e, and f). These IR bands are characteristic vibrations of ammonium hydroxide [31]. We attribute these spectral features to the chemisorption of water to the APTES amine (R-NH_2) group to form ammonium hydroxide (R-NH_3OH) and hydrogen bonding. These bands are stronger at lower temperature (100 °C) because the APTES surface density and water adsorption capacity are higher at lower temperatures. These ammonium species are likely to form when the APTES terminated surface is exposed to ambient conditions from reaction with atmospheric water vapor. However, ammonium nitrogen was not observed in the XPS spectra (Fig. 2e), because the XPS measurements are performed under ultrahigh vacuum conditions (<5 10^{-10} bar), where any adsorbed H_2O would likely desorb from the surface.

3.3. The APTES reaction on TiO_2 and ZnO

It is instructive to examine the APTES functionalization of ALD TiO_2 and ZnO surfaces since these materials are commercially significant and can be prepared by ALD with relative ease. We first conducted in situ QCM studies of TiO_2 and ZnO ALD at 100 °C and 200 °C followed by vapor phase grafting of APTES. The in situ QCM measurements of the TiO_2 and ZnO ALD are shown in Figs. S8–S15 and reveal steady-state growth of ~20 ng cm^{-2} per cycle at 100 °C and ~18 ng cm^{-2} per cycle at 200 °C for TiO_2, and ~110 ng cm^{-2} per cycle at 100 °C and ~90 ng cm^{-2} per cycle at 200 °C for ZnO, in agreement with previous studies [32,33]. Fig. 5a shows the in situ QCM measurements recorded during APTES exposures to the ALD ZnO surface at 100 °C (blue trace) and 200 °C (black trace). In both cases, the mass is seen to saturate following 1–2 APTES exposures indicating that the APTES reaction is self-limiting on the hydroxylated ZnO surface. The saturated mass gain is higher at 100

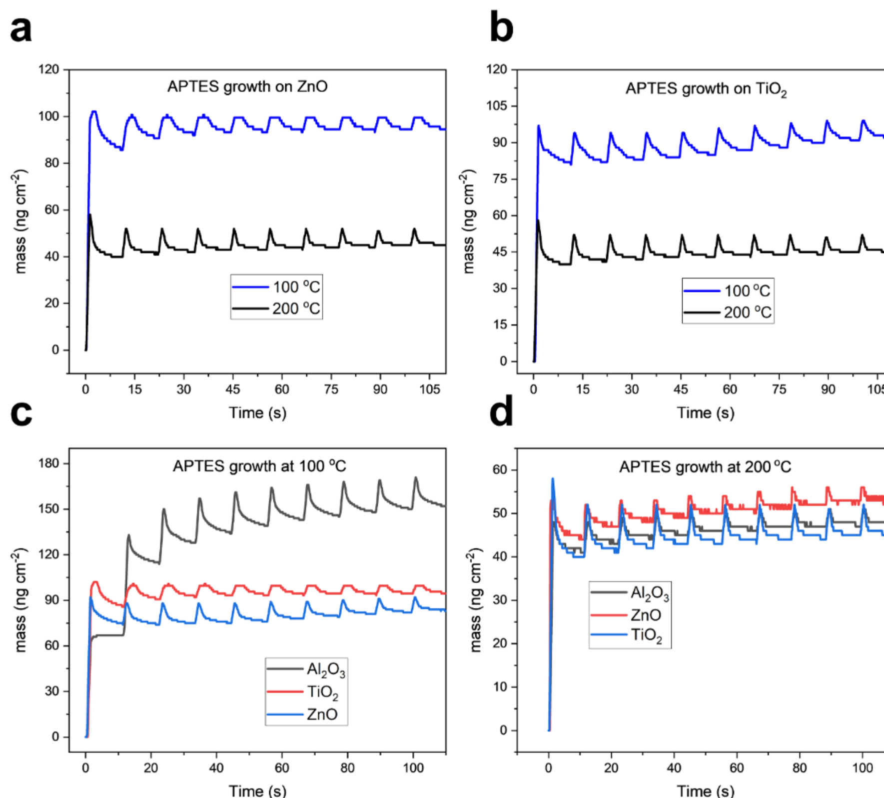

°C (93.7 ng/cm^2) compared to 200 °C (53.7 ng cm^{-2}) (Fig. 5a, Table 1). Similarly, the APTES grafting reaction saturates after 1–2 exposures on the hydroxylated ALD TiO_2 surface (Fig. 5b), and the saturation mass gain is higher 100 °C (85.7 ng cm^{-2}) compared to 200 °C (45.7 ng cm^{-2}) (Fig. 5b, Table 1). Both TiO_2 and ZnO show ~2× higher mass gain from APTES grafting at 100 °C compared to 200 °C and this trend is similar to the mass gains observed on Al_2O_3 at these temperatures. Fig. 5c shows the QCM mass versus time recorded during APTES exposures at 100 °C on Al_2O_3, TiO_2 and ZnO, and Fig. 5d shows the corresponding QCM measurements recorded at 200 °C. The QCM mass gains during APTES exposure at 200 °C are in the range of 46–54 ng cm^{-2} for all three oxides, but at 100 °C the QCM mass gain during APTES exposure on Al_2O_3 (151.3 ng cm^{-2}) is significantly higher than on ZnO (93.7 ng cm^{-2}) and TiO_2 (85.7 ng cm^{-2}). This might result from the higher surface OH density on Al_2O_3 (10.0 OH nm^{-2}) compared to ZnO (8.2 OH nm^{-2}) and TiO_2 (5.6 [34]) (Table 2), or to a different reactivity of APTES on Al_2O_3 compared to the other oxides.

To investigate the origin for the different mass loading behavior of APTES on Al_2O_3 compared to ZnO and TiO_2, we performed in situ FTIR measurements during APTES exposures on ZnO and analyzed APTES-grafted ALD ZnO samples using XPS. In Fig. 6a-b, we compare the FTIR spectra following APTES exposure to hydroxylated ZnO at 100 °C (green traces) with the corresponding measurements on hydroxylated Al_2O_3 (blue traces). The ZnO and Al_2O_3 spectra were normalized based on the RNH_2 bending bands at 1590 cm^{-1}. Consequently, the magnitudes of the other spectral features (e.g. O—H, C—H) should be directly comparable on a per-APTES molecule basis. This normalization to the RNH_2 bending band is justified only if the N atoms are present in the same configuration for both ZnO and Al_2O_3. The XPS spectra of APTES grafted Al_2O_3 showed only one type of nitrogen binding at about 400 eV (Fig. 2e) that we attribute to the RNH_2 nitrogen of APTES, and one type of silicon binding at 102 eV that we assigned to the silane silicon (Fig. 3f). Similarly, the XPS spectrum of APTES grafted ZnO showed only one type of nitrogen binding at about 400 eV (Fig. 6c) and one type of silicon bonding at 102 eV (Fig. 6d). The C1s XPS spectra for APTES grafted to both Al_2O_3 and ZnO show a large carbon peak at 284.8 eV and small shoulder peaks at 288.2 eV for Al_2O_3 (Fig. 2f) and 288.5 eV for ZnO (Fig. 6e). These shoulder peaks may derive from adventitious carbon. The XPS data indicate that APTES binds to ZnO through siloxane bonds in a similar fashion to Al_2O_3. This similarity justifies our normalization of the FTIR spectra in Fig. 6a–b.

Fig. 6a shows that the peak in the ZnO—H stretching band appears at lower frequency (3650 cm^{-1}) compared to the AlO—H stretching band (3730 cm^{-1}) (Fig. 3a). By comparing the integrated area of the ZnO—H feature before and after the APTES reaction, we found that at 100 °C only 50% of the ZnO—H react with APTES compared to 62% of the AlO—H at 100 °C (Table 2 and Fig. S17). Although these spectra were normalized based on the RNH_2 bending band at 1590 cm^{-1}, the RNH_2 stretching peak at 3265 cm^{-1} is slightly larger for ZnO compared to Al_2O_3 (Fig. 6a). This is an artifact from the lower ZnO surface OH reactivity compared to Al_2O_3, which causes the decrease in ZnO—H intensity to have less of a diminishing effect on the nearby RNH_2 stretching band. The bands at 2800–3000 cm^{-1}, characteristic of the C—H stretches in the APTES ethoxide ligands, show a similar intensity and peak distribution for both Al_2O_3 and ZnO. This demonstrates that the APTES grafted to both Al_2O_3 and ZnO have a similar distribution of unreacted ethoxides and consequently they bind in a similar fashion. In the case of Al_2O_3, we believe this binding to be a mixture of one- and two-anchored bindings. We therefore expect that APTES binds to the hydroxylated ZnO surface as a mixture of one- and two-anchored bindings. We calculated the number density of aminosilane molecules grafted to the ALD ZnO surface to be 3.36 molecules nm^{-2} at 100 °C. This is 61% lower than on the ALD Al_2O_3, possibly due to the lower surface OH density and lower reactivity of ZnO (Table 2).

We next considered the reaction of APTES with hydroxylated TiO_2. Our XPS measurements showed that APTES reacts with hydroxylated TiO_2 in a different way compared to Al_2O_3 and ZnO. For TiO_2, in addition to the N 1s XPS peak for RNH_2 nitrogen at about 400 eV, the XPS measurements revealed the formation of ammonium (RNH_3X) nitrogen at about 402 eV (Fig. 7d). The ammonium nitrogen constitutes 59% of

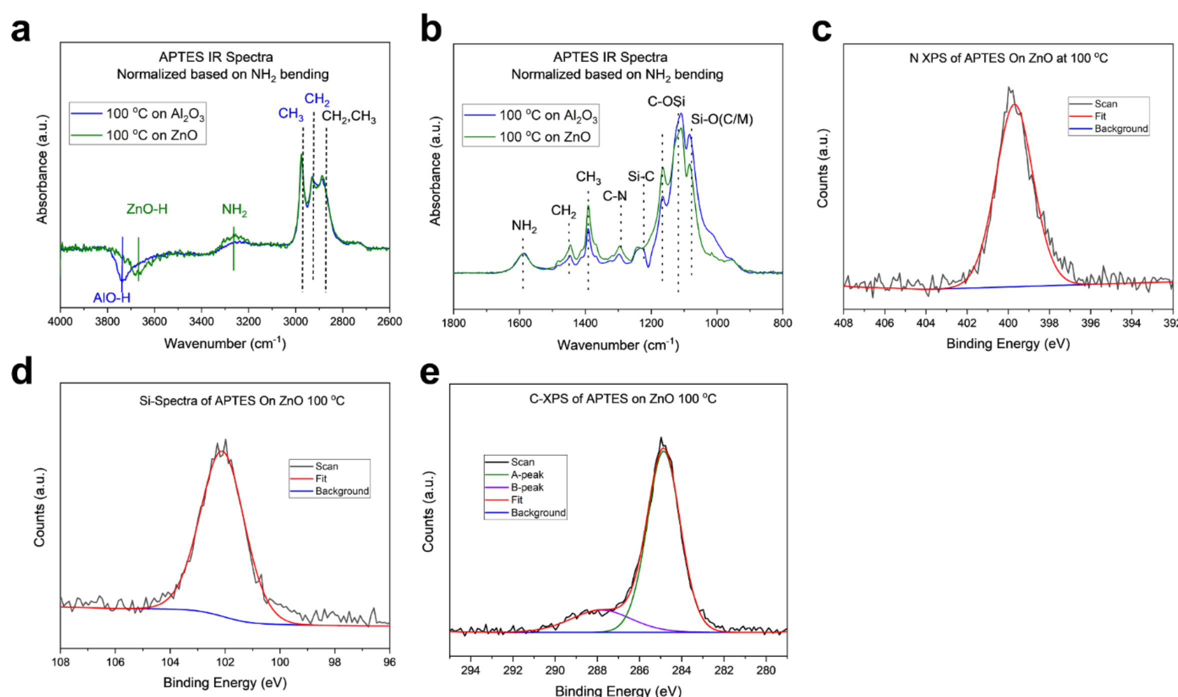

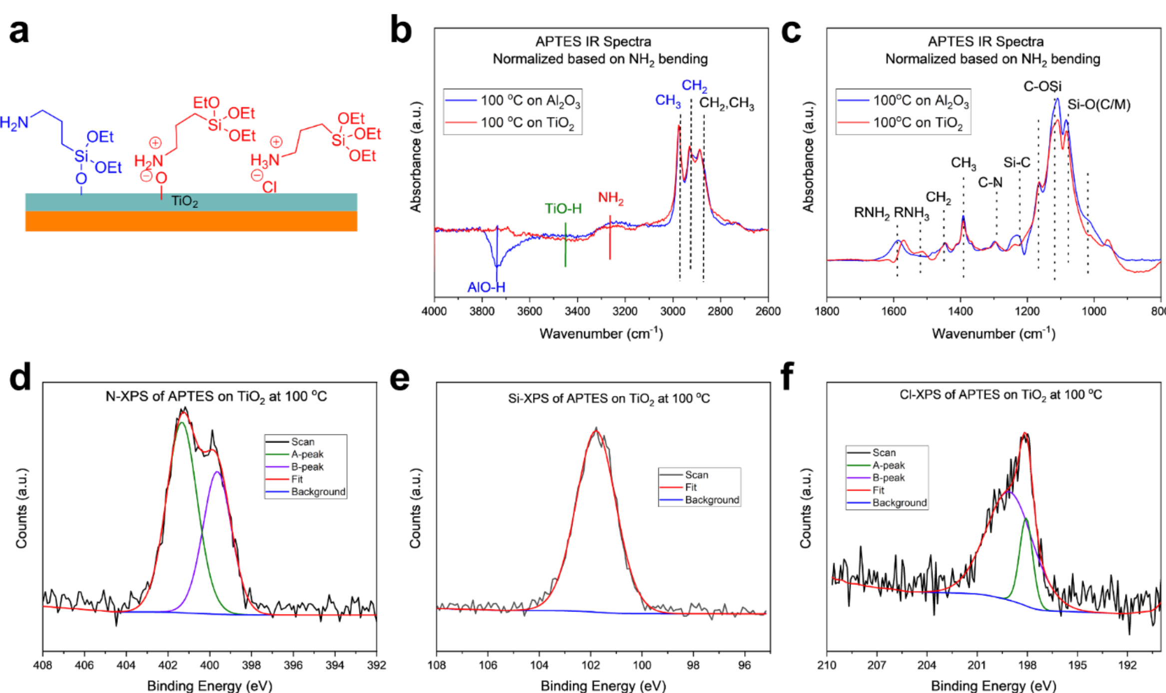

Fig. 7. APTES functionalization of TiO_2. (a) Proposed APTES binding on TiO_2. (b, c) Saturated FTIR spectra comparison of APTES reacted TiO_2 at 100 °C (red) and Al_2O_3 at 100℃ (blue), two spectra were normalized based on NH_2 bending spectra. (d) Nitrogen XPS, (e) Silicon XPS, (f) Chlorine XPS spectra of APTES reacted TiO_2 at 100 °C.

Table 3
XPS elemental composition analysis of silanized oxides.

Substrate	Temperature	N (at. %)	Si (at. %)	C (at. %)	O (at. %)	Al/Zn/Ti (at. %)	Cl (at. %)
Al_2O_3	100 °C	2.52	2.41	16.00	51.99	27.08	–
Al_2O_3	150 °C	1.84	1.82	11.40	53.04	31.90	–
Al_2O_3	200 °C	1.83	1.82	11.72	52.45	32.17	–
ZnO	100 °C	1.38	1.36	13.46	43.26	40.54	–
TiO_2	100 °C	4.07	4.44	22.20	47.74	20.40	1.15

the total N 1s XPS intensity, showing that a majority of APTES reacts through ionic binding. XPS measurements also detected chlorine (Fig. 7f and Table 3) at ~1% that we attribute to unreacted Cl from the $TiCl_4$ precursor. Residual chlorine is common in ALD TiO_2 coatings prepared using $TiCl_4$ and H_2O at lower temperatures [33]. The residual chlorine may be the reason for ionic bonding through ammonium chloride salt formation (Fig. 7a). However, given that the chlorine concentration is only 28% of the total nitrogen content, this does not account for the 59% ammonium nitrogen formation (Table 3). It has been reported that in the APTES functionalization of sputter deposited TiO_2 coatings, which do not contain residual chlorine, XPS measurements detect both amine (RNH_2) nitrogen and ammonium (RNH_3) nitrogen [18]. This different bonding configuration for APTES on TiO_2 compared to Al_2O_3 and ZnO may result from the higher acidity of surface TiO_2 protons (isoelectric pH point = 5–6) as compared to Al_2O_3 and ZnO (isoelectric pH point = 9–10) [35–38]. We believe that in our experiments, APTES reacts with TiO_2 to form both ammonium chloride and ammonium oxide as illustrated in Fig. 7a. Fig. 7b and c show FTIR measurements in the high and low frequency regions, respectively, following APTES exposure to hydroxylated TiO_2 at 100 °C (red traces) with the corresponding measurements on hydroxylated Al_2O_3 (blue traces). The FTIR spectra on through RNH_3. Ammonium also shows a broad stretching band between 3000 cm^{-1} and 3600 cm^{-1}, diminishing the negative TiO—H peak, making it difficult to quantify the number of TiO_2 hydroxyls that react with APTES. Nonetheless, assuming that APTES reacts as shown in Fig. 7a, we calculated the number density of aminosilane grafted to the ALD TiO_2 surface at 100 °C from the XPS and QCM data to be 2.55 molecules nm^{-2}. This value is lower than the number densities calculated for the ALD Al_2O_3 and ZnO surfaces, and this difference may result from the lower reactivity of TiO_2 compared to Al_2O_3 and ZnO.

3.4. The H_2O reaction on APTES-terminated TiO_2 and ZnO

Finally, we examined the reaction of H_2O with the APTES-terminated TiO_2 and ZnO surfaces using in situ QCM and FTIR measurements. The effect of H_2O exposure on the APTES-terminated ZnO was similar to that observed for the APTES-terminated Al_2O_3. The QCM measurements showed a mass loss at 100 °C of −11.5 ng cm^{-2}, and a mass loss at 200 °C of −3.7 ng cm^{-2} (Table 1 and Fig. 8a). The in situ FTIR measurements following H_2O exposure on the APTES-terminated ZnO shows a loss in C—H absorption features (3050–2950 cm^{-1}) consistent with hydrolysis of the ethoxide ligands (red trace in Fig. 8c). However, the magnitude of these changes indicates that only a small fraction (47%) of the ethoxide ligands are removed suggesting that the hydrolysis reaction does not proceed to completion at 100 °C (see Fig. S22 and Table S2 for details). In addition to the loss in ethoxide spectral features, Fig. 8c also shows the creation of siloxane (Si—O—Si) bonds at ~ 1020 cm^{-1}, and the formation of RNH_3OH as evidenced by new bands at 1540 cm^{-1} and 1630 cm^{-1} and a broad peak starting from 3800 cm^{-1} extending to 2600 cm^{-1} following H_2O reaction. These changes are similar to the changes observed following H_2O exposure to APTES-terminated Al_2O_3 (Fig. 8b).

For the case of TiO_2, unlike other oxides, in situ QCM measurements

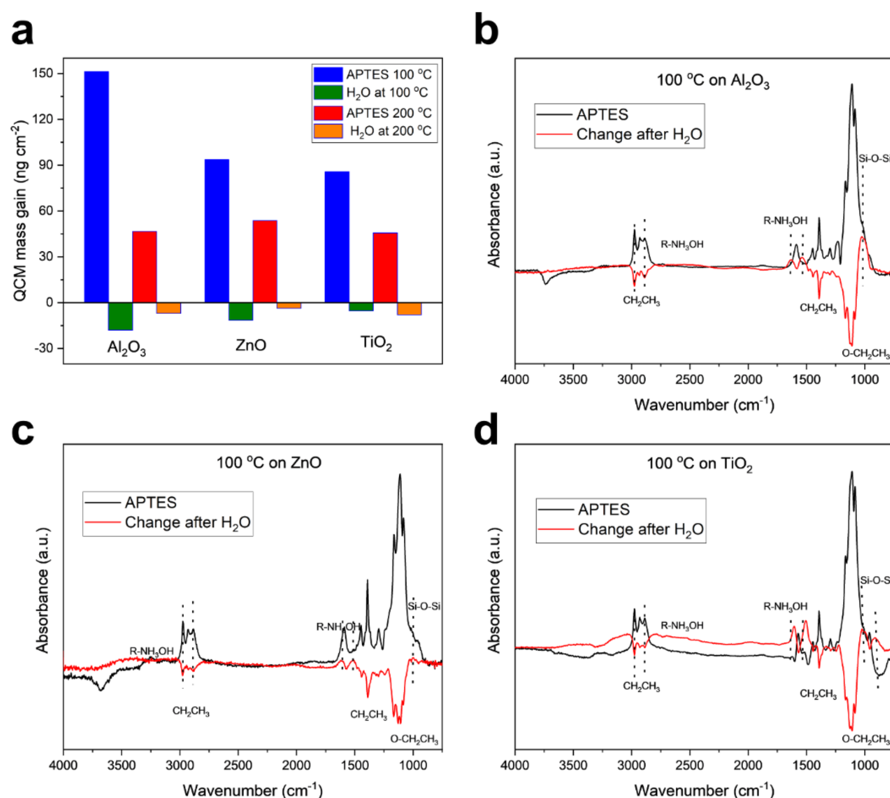

Fig. 8. (a) Comparison of QCM mass change profile of APTES reaction on Al_2O_3, ZnO and TiO_2 at 200 °C. (b) Comparison of FTIR spectra before (black) and after (blue) water exposure of APTES reacted 100 °C of APTES reacted Al_2O_3 (c) ZnO, (d) TiO_2, red spectrum was obtained by subtracting black spectrum from blue.

(59%) binds to the surface through the ammonium group, leaving the ethoxy ligands exposed to the incoming H_2O. The greater H_2O reactivity at higher temperatures and the availability of exposed ethoxy ligands might lead to a greater mass loss upon H_2O exposure at 200 °C. In FTIR, apart from ammonium hydroxide (RNH_3OH) bands, two bands were observed 1020 cm^{-1} and 920 cm^{-1}. These bands can be attributed to two different Si—O—Si bonds. Three unreacted ethoxysilanes per each ionic bonded APTES could form multiple Si—O—Si bonds, which is responsible for two different bands. Hydrolysis of ethoxides can be observed through the disappearance of characteristic C—H stretching at 2800–3000 cm^{-1}, C—H bending at 1300 cm^{-1}, and C—O stretching at 1100 cm^{-1} (Fig. 8d). When the CH_3 band (2950–3050 cm^{-1}) on TiO_2 of Fig. 8d is compared with Fig. 8c, we observe similar fraction of ethoxide removal (48%) to ZnO (see Fig. S22 and Table S2 for details). However, in Fig. 8a and Table 1, the mass decrease at 100 °C on TiO_2 (−6.2%) is lower than on ZnO (−12.3%). This could be explained by the hygroscopic property of ammonium salts [39,40]. Since mass changes result from both ethoxide removal and water adsorption, we believe this is a result of higher water adsorption to the alkylammonium species on TiO_2, which causes the lower mass decrease. This is supported by a higher broad peak around 2600–3700 cm^{-1} on TiO_2 which is characteristic of H_2O adsorbed on ammonium salts [41].

4. Conclusions

We have performed a detailed study of the vapor-phase silanization of ALD Al_2O_3, ZnO and TiO_2 surfaces using (3-aminopropyl)triethoxysilane (APTES), and the subsequent reaction of the silanized surface with H_2O vapor at temperatures between 100 °C and 200 °C. In all cases, we observed the self-limiting chemisorption of APTES to form sub-

situ XPS and AFM measurements, we established that APTES reacts with hydroxylated Al_2O_3 via one- and two-anchored siloxy (Al—O—Si) bonding at 100 °C, and two- and three-anchored siloxy bonding at 200 °C. Subsequent reaction with H_2O vapor releases only a portion of the residual ethoxy groups and forms siloxane (Si—O—Si) species at 100 °C. At 200 °C, the H_2O reaction eliminates all of the residual ethoxy groups but forms silanol groups (Si-OH) rather than siloxane species. Similar behaviors were observed for APTES reaction on ZnO surfaces, but on the TiO_2 surfaces a majority of the APTES reacted via the terminal amine group to form ionic bonds with the TiO_2 surface. This different bonding configuration for APTES on TiO_2 compared to Al_2O_3 and ZnO may result from the higher acidity of surface TiO_2 protons compared to Al_2O_3 and ZnO. Our results demonstrate that vapor-phase grafting of APTES to metal oxide surfaces is well controlled and eliminates many of the complications reported for solution phase grafting of APTES. The ability to tailor the APTES surface coverage and bonding mode by tuning the composition of the underlying metal oxide by ALD may enable the synthesis of effective sorbents for the selective removal of contaminants from water.

CRediT authorship contribution statement

Vepa Rozyyev: Writing - original draft, Writing - review & editing. **Julia G. Murphy:** Writing - review & editing. **Edward Barry:** Conceptualization, Writing - review & editing. **Anil U. Mane:** Writing - review & editing. **S.J. Sibener:** Writing - review & editing. **Jeffrey W. Elam:** Conceptualization, Writing - review & editing.

Declaration of Competing Interest

the work reported in this paper.

Acknowledgments

This work was supported as part of the Advanced Materials for Energy-Water Systems (AMEWS) Center, an Energy Frontier Research Center funded by the US Department of Energy, Office of Science, Basic Energy Sciences. AFM measurements were supported by the NSF-Materials Research Science and Engineering Center at The University of Chicago, grant no. NSF-DMR-14-20709.

Appendix A. Supplementary material

Supplementary data to this article can be found online at https://doi.org/10.1016/j.apsusc.2021.149996.

References

[1] H.N. Phong Vo, H.H. Ngo, W. Guo, T.M. Hong Nguyen, J. Li, H. Liang, L. Deng, Z. Chen, T.A. Hang Nguyen, Poly-and perfluoroalkyl substances in water and wastewater: A comprehensive review from sources to remediation, Journal of Water, Process Eng. 36 (2020), 101393.
[2] T. Guo, M.-S. Yao, Y.-H. Lin, C.-W. Nan, A comprehensive review on synthesis methods for transition-metal oxide nanostructures, CrystEngComm 17 (2015) 3551–3585.
[3] R. Sui, P. Charpentier, Synthesis of Metal Oxide Nanostructures by Direct Sol-Gel Chemistry in Supercritical Fluids, Chem. Rev. 112 (2012) 3057–3082.
[4] S. Deng, M. Kurttepeli, D.J. Cott, S. Bals, C. Detavernier, Porous nanostructured metal oxides synthesized through atomic layer deposition on a carbonaceous template followed by calcination, J. Mater. Chem. A 3 (2015) 2642–2649.
[5] M. Ritala, K. Kukli, A. Rahtu, P.I. Räisänen, M. Leskelä, T. Sajavaara, J. Keinonen, Atomic Layer Deposition of Oxide Thin Films with Metal Alkoxides as Oxygen Sources, Science 288 (2000) 319–321.
[6] M. Terracciano, I. Rea, J. Politi, L. De Stefano, Optical characterization of aminosilane-modified silicon dioxide surface for biosensing, J. Eur. Opt. Soc. - Rapid Publ. 8 (2013).
[7] A.K. Kushwaha, M.C. Chattopadhyaya, Surface modification of silica gel for adsorptive removal of Ni2+ and Cd2+ from water, Desalin. Water Treat. 54 (2015) 1642–1650.
[8] A. Liberman, N. Mendez, W.C. Trogler, A.C. Kummel, Synthesis and surface functionalization of silica nanoparticles for nanomedicine, Surf. Sci. Rep. 69 (2014) 132–158.
[9] H.A. Patel, J. Byun, C.T. Yavuz, Carbon Dioxide Capture Adsorbents: Chemistry and Methods, ChemSusChem 10 (2017) 1303–1317.
[10] S.P. Pujari, L. Scheres, A.T.M. Marcelis, H. Zuilhof, Covalent Surface Modification of Oxide Surfaces, Angew. Chem. Int. Ed. 53 (2014) 6322–6356.
[11] M. Zhu, M.Z. Lerum, W. Chen, How To Prepare Reproducible, Homogeneous, and Hydrolytically Stable Aminosilane-Derived Layers on Silica, Langmuir 28 (2012) 416–423.
[12] F. Zhang, K. Sautter, A.M. Larsen, D.A. Findley, R.C. Davis, H. Samha, M.R. Linford, Chemical Vapor Deposition of Three Aminosilanes on Silicon Dioxide: Surface Characterization, Stability, Effects of Silane Concentration, and Cyanine Dye Adsorption, Langmuir 26 (2010) 14648–14654.
[13] E.T. Vandenberg, L. Bertilsson, B. Liedberg, K. Uvdal, R. Erlandsson, H. Elwing, I. Lundström, Structure of 3-aminopropyl triethoxy silane on silicon oxide, J. Colloid Interface Sci. 147 (1991) 103–118.
[14] S. Ek, E.I. Iiskola, L. Niinistö, Gas-Phase Deposition of Aminopropylalkoxysilanes on Porous Silica, Langmuir 19 (2003) 3461–3471.
[15] A.R. Yadav, R. Sriram, J.A. Carter, B.L. Miller, Comparative study of solution-phase and vapor-phase deposition of aminosilanes on silicon dioxide surfaces, Mater. Sci. Eng. C Mater. Biol. Appl. 35 (2014) 283–290.
[16] D. Meroni, L. Lo Presti, G. Di Liberto, M. Ceotto, R.G. Acres, K.C. Prince, R. Bellani, G. Soliveri, S. Ardizzone, A Close Look at the Structure of the TiO(2)-APTES Interface in Hybrid Nanomaterials and Its Degradation Pathway: An Experimental and Theoretical Study, J. Phys. Chem. C Nanomater. Interfaces 121 (2017) 430–440.
[17] D.G. Kurth, T. Bein, Thin Films of (3-Aminopropyl)triethoxysilane on Aluminum Oxide and Gold Substrates, Langmuir 11 (1995) 3061–3067.
[18] D. Meroni, L. Lo Presti, G. Di Liberto, M. Ceotto, R.G. Acres, K.C. Prince, R. Bellani, G. Soliveri, S. Ardizzone, A Close Look at the Structure of the TiO2-APTES Interface in Hybrid Nanomaterials and Its Degradation Pathway: An Experimental and Theoretical Study, J. Phys. Chem. C 121 (2017) 430–440.
[19] S. Villa, P. Riani, F. Locardi, F. Canepa, Functionalization of Fe_3O_4 NPs by Silanization: Use of Amine (APTES) and Thiol (MPTMS) Silanes and Their Physical Characterization, Materials (Basel) 9 (2016) 826.
[20] S.M. George, Atomic Layer Deposition: An Overview, Chem. Rev. 110 (2010) 111–131.
[21] J.W. Elam, J.A. Libera, T.H. Huynh, H. Feng, M.J. Pellin, Atomic Layer Deposition of Aluminum Oxide in Mesoporous Silica Gel, J. Phys. Chem. C 114 (2010) 17286–17292.
[22] J.W. Elam, D. Routkevitch, P.P. Mardilovich, S.M. George, Conformal Coating on Ultrahigh-Aspect-Ratio Nanopores of Anodic Alumina by Atomic Layer Deposition, Chem. Mater. 15 (2003) 3507–3517.
[23] J.W. Elam, M.D. Groner, S.M. George, Viscous flow reactor with quartz crystal microbalance for thin film growth by atomic layer deposition, Rev. Sci. Instrum. 73 (2002) 2981–2987.
[24] J.D. Ferguson, A.W. Weimer, S.M. George, Atomic layer deposition of ultrathin and conformal Al2O3 films on BN particles, Thin Solid Films 371 (2000) 95–104.
[25] R.M. Pasternack, S. Rivillon Amy, Y.J. Chabal, Attachment of 3-(Aminopropyl) triethoxysilane on Silicon Oxide Surfaces: Dependence on Solution Temperature, Langmuir 24 (2008) 12963–12971.
[26] J.W. Elam, D. Routkevitch, S.M. George, Properties of ZnO/Al[sub 2]O[sub 3] Alloy Films Grown Using Atomic Layer Deposition Techniques, J. Electrochem. Soc. 150 (2003) G339.
[27] Y. Huang, G. Pandraud, P.M. Sarro, Characterization of low temperature deposited atomic layer deposition TiO2 for MEMS applications, J. Vac. Sci. Technol., A 31 (2013) 01A148.
[28] R.J.J. Jansen, H. van Bekkum, XPS of nitrogen-containing functional groups on activated carbon, Carbon 33 (1995) 1021–1027.
[29] L.T. Zhuravlev, The surface chemistry of amorphous silica. Zhuravlev model, Colloids Surf. A: Physicochem. Eng. Aspects 173 (2000) 1–38.
[30] R.L. Puurunen, M. Lindblad, A. Root, A.O.I. Krause, Successive reactions of gaseous trimethylaluminum and ammonia on porous alumina, PCCP 3 (2001) 1093–1102.
[31] P.P. Sethna, H.D. Downing, L.W. Pinkley, D. Williams, Infrared band intensities in ammonium hydroxide and ammonium salts, J. Opt. Soc. Am. 68 (1978) 429–431.
[32] J. Cai, Z. Ma, U. Wejinya, M. Zou, Y. Liu, H. Zhou, X. Meng, A revisit to atomic layer deposition of zinc oxide using diethylzinc and water as precursors, J. Mater. Sci. 54 (2019) 5236–5248.
[33] J. Aarik, A. Aidla, H. Mändar, T. Uustare, Atomic layer deposition of titanium dioxide from TiCl4 and H2O: investigation of growth mechanism, Appl. Surf. Sci. 172 (2001) 148–158.
[34] R. Mueller, H.K. Kammler, K. Wegner, S.E. Pratsinis, OH Surface Density of SiO2 and TiO2 by Thermogravimetric Analysis, Langmuir 19 (2003) 160–165.
[35] J.J. Gulicovski, L.S. Čerović, S.K. Milonjić, Point of Zero Charge and Isoelectric Point of Alumina, Mater. Manuf. Processes 23 (2008) 615–619.
[36] S. Liufu, H. Xiao, Y. Li, Investigation of PEG adsorption on the surface of zinc oxide nanoparticles, Powder Technol. 145 (2004) 20–24.
[37] C. Pfeiffer, C. Rehbock, D. Hühn, C. Carrillo-Carrion, D.J.d Aberasturi, V. Merk, S. Barcikowski, W.J. Parak, Interaction of colloidal nanoparticles with their local environment: the (ionic) nanoenvironment around nanoparticles is different from bulk and determines the physico-chemical properties of the nanoparticles, J. R. Soc. Interface 11 (2014) 20130931.
[38] M. Sugiyama, H. Okazaki, S. Koda, Size and Shape Transformation of TiO2Nanoparticles by Irradiation of 308-nm Laser Beam, Jpn. J. Appl. Phys. 41 (2002) 4666–4674.
[39] D. Hu, J. Chen, X. Ye, L. Li, X. Yang, Hygroscopicity and evaporation of ammonium chloride and ammonium nitrate: Relative humidity and size effects on the growth factor, Atmos. Environ. 45 (2011) 2349–2355.
[40] P.G. Hall, M.A. Rose, Adsorption of water vapor on ammonium iodide and ammonium chloride, J. Phys. Chem. 82 (1978) 1521–1525.
[41] M.A. Zawadowicz, S.R. Proud, S.S. Seppalainen, D.J. Cziczo, Hygroscopic and phase separation properties of ammonium sulfate/organics/water ternary solutions, Atmos. Chem. Phys. 15 (2015) 8975–8986.